Magneto-resistance study of AFe_2As_2 (A = Sr, Ba) iron-based compounds

S.V. Chong*

Callaghan Innovation Research Limited, P.O. Box 31310,
Lower Hutt, New Zealand
Fax: +64-4-9313117
E-mail: shen.chong@callaghaninnovation.govt.nz
*Corresponding author

G.V.M. Williams

MacDiarmid Institute,
School of Chemical and Physical Sciences, Victoria University of Wellington,
P.O. Box 600, Wellington, New Zealand
Fax: +64-4-4635241
E-mail: Grant.Williams@vuw.ac.nz

S. Sambale

Callaghan Innovation Research Limited, P.O. Box 31310,
Lower Hutt, New Zealand and
MacDiarmid Institute,
School of Chemical and Physical Sciences, Victoria University of Wellington,
P.O. Box 600, Wellington, New Zealand
Fax: +64-4-9313117
E-mail: Sebastian.Sambale@vuw.ac.nz

J. Kennedy

National Isotope Centre, GNS Science,
P.O. Box 31312, Lower Hutt, New Zealand
Fax: +64-4-5704657
E-mail: J.Kennedy@gns.cri.nz

K. Kadowaki

Institute of Materials Science, University of Tsukuba,
1-1-1, Tennodai, Tsukuba, Ibaraki, Japan
Fax: +81-298-557440
E-mail: k.kadowaki@ims.tsukuba.ac.jp

Abstract

We have investigated the magneto-resistance (MR) from the two main AFe_2As_2 compounds (with A = Sr and Ba) and a low energy Ca ion implanted $SrFe_2As_2$ crystal up to 8 T. We show that MR from $BaFe_2As_2$ and $SrFe_2As_2$ single crystals are similar and a quantum linear MR model favoured by some authors is probably not appropriate especially since the MR is not linear. The $SrFe_2As_2$ sample with a near surface Ca concentration of 0.8 at.% has a larger MR at low temperatures that is probably due to current transport in the near surface region and in an inhomogeneous normal and superconducting state.

Keywords: iron-pnictides; superconductivity; magneto-resistance; Dirac fermions; quantum linear magneto-resistance.

1. Introduction

The recently discovered high-temperature superconducting iron-based compounds, with a superconducting transition temperature as high as 56 K, are known to be unconventional superconductors, with a notable feature that a single-carrier model is inadequate to characterise their transport behaviour due, for example, to the multiband nature of the d-orbitals involved in the conduction bands [1–4]. Furthermore, they also possess several interesting practical properties such as a sizeable thermo-electric effect [5, 6], a large magneto-resistance (MR) [7,8], and a Dirac-cone-like energy dispersion, which is caused by band crossing as revealed by ARPES and quantum oscillation measurements [9,10]. The last feature is particularly interesting because it can lead to Dirac fermions with very high mobilities and a nearly zero effective mass, m* [9–13]. At sufficiently high fields and if the Fermi level is close to the cone apex then a Dirac-cone-like energy dispersion can lead to a quantum linear MR. This was predicted by Abrikosov where the resistivity can be written as $\rho_{xx} = \rho_{yy} = [N_i/(\pi n_D^2 e)] \times B$ (N_i is the concentration of static scattering centres, and n_D is the density of carriers, and B is the applied magnetic field) [14]. There have been a few reports from magneto-transport measurements on the 1111- and 122-iron-arsenides [11–13] families of the iron-pnictides that a quantum linear MR has been observed. However, it has been argued that the fields required to observe a quantum linear MR in $BaFe_2As_2$ are too high [15] and that a quantum linear MR is not observed in good quality and homogeneous samples [7]. We have recently shown that very high magneto-resistances are observed in a $SrFe_2As_2$ crystal that was left in a desiccator for 7 months and the conduction pathway was through normal and superconducting regions [8]. However, the MR data are more consistent with multi-band transport and the MR is not dominated by quantum linear magneto-transport. Clearly more studies are required, and for this reason we have measured the MR from non-superconducting $BaFe_2As_2$ and $SrFe_2As_2$, and report our results in this paper. We also report the results from MR measurements on a low energy Ca ion implanted $SrFe_2As_2$ sample to see if this can induce a large MR similar to the more than 1600% MR observed in a $SrFe_2As_2$ sample that displayed an inhomogeneous mixed phase containing superconducting and normal state regions [8].

2. Experimental details

$BaFe_2As_2$ and $SrFe_2As_2$ single crystals were prepared by the self-flux method using excess FeAs following the literature method [16,17]. Platelet crystals were mechanically cleaved off from the obtained solidified melt and show sharp c-axis (00l) Bragg reflections in powder X-ray diffraction. The samples were stored in a desiccator and measured less than one month after synthesis. The $SrFe_2As_2$ single crystalline sample used for ion implantation experiments were from our previous study[18]. Calcium ion-implantation was carried out at the GNS Science ion implantation facility using a 20 keV beam energy, similar to our previous work [19]. The implantation was carried out on both surfaces of a ~46 μm thick crystal, along the c-axis with the same fluences. An estimated implantation depth of 10–15 nm was determined from a Monte Carlo simulation [20]. The fluence of 1×10^{15} ions/cm^2 corresponds to an average Ca concentration in the implanted region of 0.8%. The ion current was set to a low value (1 μA) to avoid heating effects during implantation. Physical characterisations were carried out on the as-prepared and as-implanted samples without subjecting them to post-annealing processes. MR measurements at various temperatures were made using the standard four-terminal configuration with the current in the ab-plane and the applied magnetic field in the c-axis using a Physical Property Measurement System.

3 Results and discussion

Figure 1(a) shows the in-plane temperature dependent resistivity for the $BaFe_2As_2$, $SrFe_2As_2$ and 0.8 at.% Ca implanted $SrFe_2As_2$ single crystals without an applied magnetic field. All three samples show a typical sharp drop in the resistivities

in the high temperature region, which is associated with the spin-density-wave (SDW) magneto-structural transition at 205 K for $SrFe_2As_2$ and 135 K for $BaFe_2As_2$. The as-prepared $BaFe_2As_2$ and $SrFe_2As_2$ samples follow a Fermi liquid T^2 behaviour and there is no evidence for a downturn in the resistivity that could signal the appearance of superconductivity. The low-energy Ca implanted $SrFe_2As_2$ crystal does show a downturn in the resistivity below ~15 K. We previously observed a downturn in the resistivity from a similar low energy Ca ion implanted $SrFe_2As_2$ crystal but the Ca concentration was 6 at.% and a downturn in the resistivity was observed at ~23.6 K and zero resistivity occurred at ~16.4 K [18]. This was attributed to strain-induced superconductivity in the near surface region that was caused by the ion implantation [18]. This interpretation was supported by hydrostatic pressure studies on non-superconducting AFe_2As_2 (A = Ba, Sr or Ca) that display a downturn in resistivity at low pressure but became superconducting as the pressure was increased [21–23]. In our case the 0.8 at.% Ca implanted crystal does not show zero resistance for temperatures as low as 2.2 K. Thus, similar to studies on 1.6 at.% K low energy ion implantation into $SrFe_2As_2$ [18], the percolation pathway in the implanted region contains superconducting and non-superconducting regions

The MR behaviour was investigated by applying magnetic fields of up to 8 T. The MR is defined as $MR = (\rho(B) - \rho(0))/\rho(0)$. The results from MR measurements on $BaFe_2As_2$ are shown in Figure 2(a). The MR is negligible above the SDW transition temperature at 135 K but increases rapidly below this. The maximum MR is ~22% at 8 T and 8 K, which is less than the maximum MR of 280% at 5 K and 7 T reported in another study [7]. For applied magnetic fields above 2 T, the MR data for all temperatures can be fitted to a power-low behaviour where $MR(B) = a_1 B^m$. We find that $m = 1.48$ at 100 K and it systematically reduces to 1.15 as the temperature is reduced to 8 K. However, the field dependence is different for low applied magnetic fields. This is apparent in the derivative of the MR plotted in Figure 2(b), where it can be seen that there is change in the MR behaviour from low to high applied magnetic fields. In the quantum linear magneto-resistance scenario, this change was attributed to a crossover from multi-band MR to quantum linear MR [11–13]. The crossover field B* has been used to estimate the Fermi velocity and Fermi energy by assuming that $\Delta_1 = k_B T + E_F$, where Δ_1 is the field-induced splitting of the first Landau level, and $\Delta_1 = \upsilon_F(2\hbar e B^*)^{1/2}$ where υ_F is the Fermi velocity and E_F is the energy of the Fermi level [12–14]. Thus, B* can be written as

$$B^* = \left(\frac{1}{2e\hbar v_F^2}\right)(k_B T + E_F).$$

A plot of B^* against temperature can then be used to estimate υ_F and E_F. This plot is shown in Figure 2(c). We find that E_F = 7.1 meV, and Fermi velocity, $\upsilon_F = 2.5 \times 10^5$ ms^{-1}. These values are similar to those deduced from measurements on $BaFe_2As_2$ [12,13] where the Dirac cone states are well documented. E_F is slightly higher than that reported from MR measurements on $BaFe_2As_2$ (2.48 meV, Huynh *et al*. [12]) but it is within the range reported from MR measurements on $Ba(Fe_{1-x}Ru_x)_2As_2$ (3–12 meV, Tanabe et al. [13]). υ_F is very similar to $\upsilon_F \sim 2 \times 10^5$ ms^{-1} reported in both studies. However, as mentioned above the MR is not linear at high fields. A similar absence of a linear MR at high fields was noted by Terashima *et al.* [15] and they argued that the field required for only one Landau level to be filled is very high and far above our maximum field of 8 T. Thus, it is highly likely that, similar to our previous study on a $SrFe_2As_2$ sample that showed superconducting and normal state regions [18], the MR is not dominated by quantum linear MR and it is probably best described using a conventional three-band transport model [8]. This is consistent with a study on $BaFe_2As_2$ crystals that were annealed to remove defects where a quantum linear MR was also not observed and it was shown that a three carrier model could describe the MR over the measured magnetic field range [7].

The MR data from our new non-superconducting $SrFe_2As_2$ crystal are plotted in Figure 3(a). The MR reaches ~31% at 2 K and 8 T, and it is slightly higher than that found for the $BaFe_2As_2$ crystal. The MR above 2 T can also

be fitted to a power-law, where m is 1.51 at 150 K and systematically reduces to 1.21 at 2 K. As can be seen in Figure 3(b) there is also an apparent MR crossover in the derivative of the MR. A fit to B^* using equation (1) gives E_F = 10 meV, and $\upsilon_F = 3 \times 10^5$ ms^{-1}, although the fit to the data is not very good. Again, it is highly likely that a three carrier model is probably more appropriate rather than a high-field quantum linear MR. Furthermore, the Fermi level appears to be too high for quantum linear MR to be observed at magnetic fields less than 8 T. The maximum MR of ~31% at 8 T and at 2 K is significantly less than that found in a previous study on a $SrFe_2As_2$ sample that was aged in a desiccator for7 months (>1600% at 10 K) [8]. However, the high MR in the previous study was attributed to MR is an inhomogeneous sample with superconducting and normal state regions, where the gradual appearance of superconductivity is likely to be due to water vapour adsorption [24] and strain [25].

The MR from the low energy 0.8 at.% Ca implanted $SrFe_2As_2$ crystal is plotted in Figure 3(c). The MR at and above 20 K is similar to that found in the non-superconducting $SrFe_2As_2$ crystal and it reaches ~24% at 20 K and 8 T. Similar to the other two crystals, the MR above 2 T can be fitted to a power law with m = 1.39 at 150 K and it reduces to 1.15 at 20 K. However, the MR at 10 K and 2 K is different where there is an initial rise in the MR. It can be more clearly seen at 2 K where it saturates at ~1 T. Furthermore, the maximum MR at 2 K and 8 T is high and it is ~47%, which is significantly larger than that found in the non-superconducting $SrFe_2As_2$ sample (~31%). The differences in the field dependence of the MR are also apparent in the derivative of the MR that is plotted in Figure 3(d). The derivatives at 2 K and 10 K are significantly larger[2]at low fields and then it decreases to a nearly constant value. The different MR behaviour at 10 K and below is likely to be caused by magneto-transport in the near surface region that contains normal and superconducting regions that are evident in the resistivity data plotted in Figure 1. As the magnetic field is increased the weak-links in the superconducting region become normal and this results in an initial increase in the MR. The MR will saturate when all of the weak-links have been driven normal by the applied field. Similar MR behaviour is also found in granular YBCO high temperature superconductors [26]. The initial increase in the MR cannot be attributed to all of the superconducting regions being driven normal because the out-of-plane upper critical field, B_c^c, for this superconductor is above 8 T below 10 K [18]. Unlike magneto-transport in weak-linked superconductors, the MR for the 0.8 at.% Ca $SrFe_2As_2$ crystal continues to increase and it is nearly linear above 1.6 T. However, we do not believe that this signals quantum linear transport. Instead, we believe that it is more likely to be due to inhomogeneous current transport in normal and superconducting regions in the near surface region. In a very simple model, the resistivity is shorted out by the superconducting regions and the MR would then be due to multi-carrier transport in the normal regions. This model has already been used to account for the bulk MR in a $SrFe_2As_2$ sample that displayed an inhomogeneous state with superconducting and normal state regions after being left in a desiccator for 7 months [8].

4 Conclusions

We have studied the MR in non-superconducting $BaFe_2As_2$ and $SrFe_2As_2$ as well as in low energy Ca implanted $SrFe_2As_2$ that displays a mixed superconducting and normal state in the near surface region. We show that while the derivative of the MR data can be analysed in terms of a crossover from classical to quantum linear MR with reasonable Fermi velocities, the field dependence of the MR is not linear as expected for quantum linear MR, and hence the MR in these compounds is unlikely to be by quantum linear MR at least below 8 T. This is also supported by a simple power law analysis on the high field MR data, which in the case of a linear MR behaviour, the exponent, m, should be 1. We found m ~ 1.5 at high temperatures and reduces to ~1.1 – 1.2 at low temperatures in the absence of superconductivity. Thus, the use of only a B^* analysis is probably not appropriate to be used as proof of quantum linear transport. The low energy Ca ion implanted sample shows an enhanced MR at low temperatures when compared to

non-superconducting $SrFe_2As_2$ and it reaches 47% at 2 K and 8 T, which is likely to be due to current transport in the near surface region and through an inhomogeneous normal and superconducting state. The large near surface MR could possibly have an application in the area of low temperature and high magnetic field sensing.

Acknowledgements

This work is supported by the Marsden Fund of New Zealand (VUW0917) and The MacDiarmid Institute for Advanced Materials and Nanotechnology. We would like to thank H. Singh (VUW) for his assistance in the data analysis.

References

1 Kamihara, Y., Watanabe, T., Hirano, M. and Hosono, H. (2008) 'Iron-based layered superconductor $La[O_{1-x}F_x]FeAs$ ($x = 0.05$-0.12) with $T_C = 26$ K', J. Am. Chem. Soc., Vol. 130, No. 11, pp.3296–3297.

2 Ishida, K., Nakai, Y. and Hosono, H. (2009) 'To what extent iron-pnictide new superconductors have been clarified: a progress report', J. Phys. Soc. Jpn., Vol. 78, No. 062001, pp.1–20.

3 Johnston, D. C. (2010) 'The puzzle of high temperature superconductivity in layered iron pnictides and chalcogenides', Adv. Phys., Vol.59, No. 6, pp.803–1061.

4 Paglione, J. and Greene, R.L. (2010) 'High-temperature superconductivity in iron-based materials', Nat. Phys., Vol. 6, No. 9, pp.645–658.

5 Pinsard-Gaudart, L., Bérardan, D., Bobroff, J. and Dragoe, N. (2008) 'Large Seebeck coefficients in iron-oxypnictides: a new route towards n-type thermoelectric materials', Phys. Status Solidi (RRL), Vol. 2, No. 4, pp.185–187; Pinsard-Gaudart, L. and Dragoe, N. (2008), 'Large thermoelectric power factor in iron-pnictide derivatives', J. Phys. Soc. Jpn. Suppl. C, Vol. 77, pp.58–60.

6 Okuda, T., Hirata, W., Takemori, A., Suzuki, S., Saijo, S., Miyasaka, S. and Tajima, S. (2011), 'Thermoelectric properties of $LaFePO_{1-x}F_x$ and $LaFeAsO_{1-x}F_x$ – Possibility of the hidden mass enhancement of $LaFeAsO_{1-x}F_x$', J. Phys. Soc. Jpn., Vol. 80, No. 044704, pp.1–8.

7 Ishida, S., Liang, T., Nakajima, M., Kihou, K., Lee, C.H., Iyo, A., Eisaki, H., Kakeshita, T., Kida, T., Hagiwara, M., Tomioka, Y., Ito, T. and Uchida, S. (2011) 'Manifestations of multiple-carrier charge transport in the magnetostructurally ordered phase of $BaFe_2As_2$', Phys. Rev. B, Vol. 84, No. 184514, pp.1–7.

8 Chong, S. V., Williams, G. V. M., Kennedy, J., Fang, F., Tallon, J. L. and Kadowaki, K. (2013), 'Large low-temperature magnetoresistance in $SrFe_2As_2$ single crystals', Europhys. Lett., Vol. 104, No. 17002, pp.1–6.

9 Richard, P., Nakayama, K., Sato, T., Neupane, M., Xu, Y-M., Bowen, J. H., Chen, G. F., Luo, J. L., Wang, N. L., Dai, X., Fang, Z., Ding, H. and Takahashi, T. (2010) 'Observation of Dirac cone electronic dispersion in $BaFe_2As_2$', Phys. Rev. Lett., Vol. 104, No. 137001, pp.1–4.

10 Sutherland M., Hills, D. J., Tan, B. S., Altarawneh, M. M., Harrison, N., Gillett, J., O'Farrell, E. C. T., Benseman, T. M., Kokanovic, I., Syers, P., Cooper, J. R. and Sebastian, S. E. (2011) 'Evidence for Dirac nodes from quantum oscillations in $SrFe_2As_2$', Phys. Rev. B, Vol. 84, No. 180506R, pp.1–5.

11 Bhoi, D., Mandal, P., Choudhury, P., Pandya, S. and Ganesan, V. (2011) 'Quantum magnetoresistance of the PrFeAsO oxypnictide', Appl. Phys. Lett., Vol. 98, No. 172105, pp.1–3); Meena, R. S., Singh, S. K., Pal, A., Kumar, A., Jha, R., Rao, K. V. R., Du, Y., Wang, X. L. and Awana, V. P. S. (2012) 'High Field (14Tesla) Magneto Transport of Sm/PrFeAsO', J. Appl. Phys., Vol. 111, No. 07E323, pp.1–3.

12 Huynh, K. K., Tanabe, Y. and Tanigaki, K. (2011) 'Both electron and hole Dirac cone states in $Ba(FeAs)_2$ confirmed by magnetoresistance', Phys. Rev. Lett., Vol. 106, No. 217004, pp.1–4.

13 Tanabe, Y., Huynh, K. K., Heguri, S., Mu, G., Urata, T., Xu, J., Nouchi, R., Mitoma, N. and Tanigaki, K. (2011)

'Coexistence of Dirac-cone states and superconductivity in iron pnictide $Ba(Fe_{1-x}Ru_xAs)_2$', Phys. Rev. B, Vol. 84, No. 100508R, pp.1–4.

14 Abrikosov, A.A. (1998) 'Quantum magnetoresistance', Phys. Rev. B, Vol. 58, No. 5, pp.2788–2794; Abrikosov, A.A. (2000) 'Quantum linear magnetoresistance', Europhys. Lett., Vol. 49, No. 6, pp.789–793.

15 Terashima, T., Kurita, N., Tomita, M., Kihou, K., Lee, C.-H., Tomioka, Y., Ito, T., Iyo, A., Eisaki, H., Liang, T., Nakajima, M., Ishida, S., Uchida, S.-I., Harima, H. and Uji, S. (2011) 'Complete Fermi surface in $BaFe_2As_2$ observed via Shubnikov–de Haas oscillation measurements on detwinned single crystals', Phys. Rev. Lett., Vol. 107, No. 176402, pp.1–5.

16 Wang, X. F., Wu, T., Wu, G., Chen, H., Xie, Y. L., Ying, J. J., Yan, Y.J., Liu, R.H. and Chen, X.H. (2009) 'Anisotropy in the electrical resistivity and susceptibility of superconducting $BaFe_2As_2$ single crystals', Phys. Rev. Lett., Vol. 102, No. 117005, pp.1–4.

17 Luo, H., Wang, Z., Yang, H., Cheng, P., Zhu, X. and Wen, H-H. (2008) 'Growth and characterization of $A_{1-x}K_xFe_2As_2$ (A = Ba, Sr) single crystals with x = 0–0.4', Supercond. Sci. Technol., Vol. 21, No. 125014, pp.1–5.

18 Chong, S. V., Tallon, J. L., Fang, F., Kennedy, J., Kadowaki, K. and Williams, G. V. M. (2011) 'Surface superconductivity on $SrFe_2As_2$ single crystals induced by ion implantation', Europhys. Lett., Vol. 94, No. 37009, pp.1–6.

19 Islah-u-din, Fox, M. R., Martin, H., Gainsford, G. J., Kennedy, J., Markwitz, A., Telfer, S. G., Jameson, G. B. and Tallon, J. L. (2010) 'Synthesis and structure of Na^+-intercalated WO_3(4,4′- bipyridyl)$_{0.5}$', Chem. Commun., Vol. 46, pp.4261–4263; Markwitz, A. and Kennedy, J. (2009), 'Group-IV and V ion implantation into nanomaterials and elemental analysis on the nanometer scale', Int. J. Nanotechnol., Vol. 6, Nos. 3–4, pp.369–383.

20 Biersack, J.P. (1987) 'Three-dimensional distributions of ion range and damage including recoil transport', Nucl. Instrum. Methods Phys. Res., Sect. B, Vols. 19–20, pp.32–39.

21 Kotegawa, H., Sugawara, H. and Tou, H. (2009) 'Abrupt emergence of pressure-induced superconductivity of 34 K in $SrFe_2As_2$: a resistivity study under pressure', J. Phys. Soc. Jpn., Vol. 78, No. 013709, pp.1–4; Colombier, E., Bud'ko, S.L., Ni, N. and Canfield, P.C. (2009), 'Complete pressure-dependent phase diagrams for $SrFe_2As_2$ and $BaFe_2As_2$', Phys. Rev. B, Vol. 79, No. 224518, pp.1–9.

22 Lee, H., Park, E., Park, T., Sidorov, V. A., Ronning, F., Bauer, E. D. and Thompson, J. D. (2009) 'Pressure-induced superconducting state of antiferromagnetic $CaFe_2As_2$', Phys. Rev. B, Vol. 80, No. 024519, pp.1–6.

23 Ishikawa, F., Eguchi, N., Kodama, M., Fujimaki, K., Einaga, M., Ohmura, A., Nakayama, A., Mitsuda, A. and Yamada, Y. (2009) 'Zero-resistance superconducting phase in $BaFe_2As_2$ under high pressure', Phys. Rev. B, Vol. 79, No. 172506, pp.1–3.

24 Hiramatsu, H., Katase, T., Kamiya, T., Hirano, M. and Hosono, H. (2009) 'Water-induced superconductivity in $SrFe_2As_2$', Phys. Rev. B, Vol. 80, No. 052501, pp.1–4.

25 Saha, S. R., Butch, N. P., Kirshenbaum, K., Paglione, J. and Zavalij, P. J. (2009), 'Superconducting and ferromagnetic phases induced by lattice distortions in stoichiometric $SrFe_2As_2$ single crystals', Phys. Rev. Lett., Vol. 103, No. 037005, pp.1–4.

26 Hamrita, A., Azzouz, F.B., Madani, A. and Salem, M.B. (2012) 'Magnetoresistivity and microstructure of $YBa_2Cu_3O_y$ prepared using planetary ball milling', Physica C, Vol. 472, No. 1, pp.34–38.

Figures

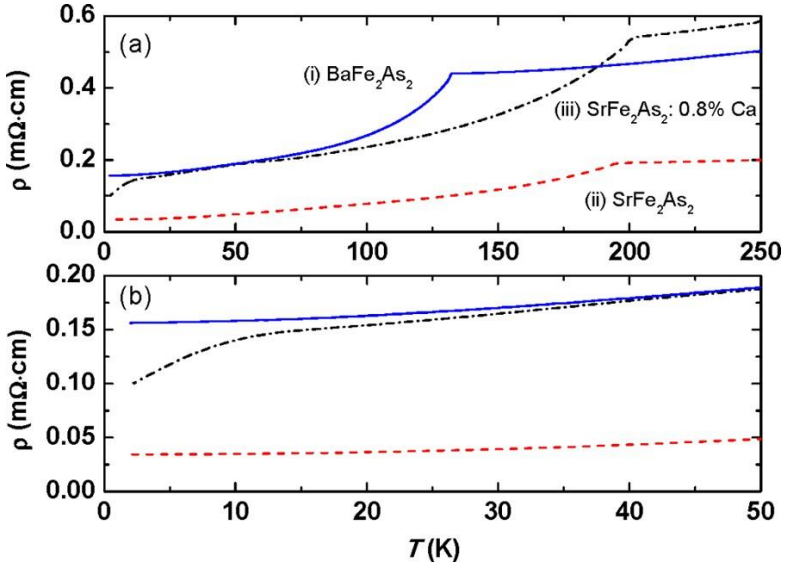

Figure 1 (a) Temperature dependent resistivity from (i) $BaFe_2As_2$ (solid curve), (ii) $SrFe_2As_2$ (dashed curve) and (iii) 0.8 at.% Ca implanted $SrFe_2As_2$, (dot-dash curve). (b) The same plot in the low temperature region (see online version or colours)

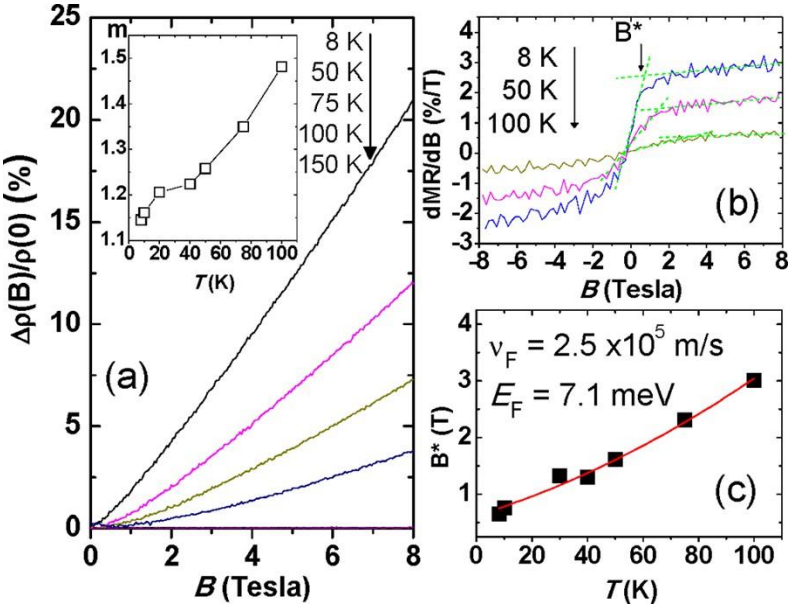

Figure 2 (a) MR from $BaFe_2As_2$. The inset shows the temperature dependence of the exponent, m, based on a power-law fit, $MR(B) = a_1(B)^m$, to the MR above 2 T. (b) Derivative of the MR for three selected temperatures. The dashed lines show the crossover field of the dMR/dB plots, where the field at the intersection of the two linear lines is defined as the crossover field, B*. (c) The corresponding temperature dependence of the crossover field. The solid curve is the fit from equation (1) (see online version or colours)

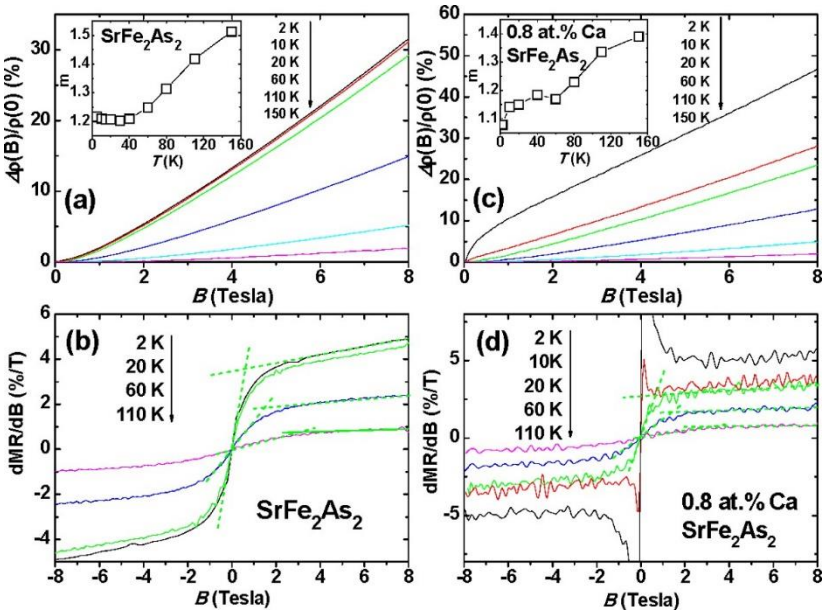

Figure 3 (a) MR from as-made $SrFe_2As_2$. (b) Plot of the corresponding derivative of the MR for several selected temperatures. The dashed lines show the crossover field of the dMR/dB plots. (c) and (d) show similar plots for the 0.8 at.% Ca implanted $SrFe_2As_2$. The insets in (a) and (c) show the temperature dependence of the exponent, m, in $MR(B) = a_1(B)^m$ obtained by fitting the MR above 2 T (see online version or colours).